1-1-2009

Vacuum-ultraviolet frequency combs from below-threshold harmonics

Dylan C. Yost
University of Colorado Boulder

Thomas R. Schibli
University of Colorado Boulder

Jun Ye
University of Colorado Boulder

Jennifer L. Tate
Louisiana State University

James Hostetter
Louisiana State University

See next page for additional authors

Recommended Citation

Yost, D., Schibli, T., Ye, J., Tate, J., Hostetter, J., Gaarde, M., & Schafer, K. (2009). Vacuum-ultraviolet frequency combs from below-threshold harmonics. *Nature Physics, 5* (11), 815-820. https://doi.org/10.1038/nphys1398

nature physics

LETTERS

PUBLISHED ONLINE: 20 SEPTEMBER 2009 | DOI: 10.1038/NPHYS1398

Vacuum-ultraviolet frequency combs from below-threshold harmonics

Dylan C. Yost[1], Thomas R. Schibli[1], Jun Ye[1]*, Jennifer L. Tate[2], James Hostetter[2], Mette B. Gaarde[2] and Kenneth J. Schafer[2]

Recent demonstrations of high-harmonic generation (HHG) at very high repetition frequencies (~100 MHz) may allow for the revolutionary transfer of frequency combs to the vacuum-ultraviolet range. This advance necessitates unifying optical frequency-comb technology with strong-field atomic physics. Whereas strong-field studies of HHG have often focused on above-threshold harmonic generation (photon energy above the ionization potential), for vacuum-ultraviolet frequency combs an understanding of below-threshold harmonic orders and their generation process is crucial. Here, we present a new and quantitative study of the harmonics 7–13 generated below and near the ionization threshold in xenon gas with an intense 1,070 nm driving field. We show multiple generation pathways for these harmonics that are manifested as on-axis interference in the harmonic yield. This discovery provides a new understanding of the strong-field, below-threshold dynamics under the influence of an atomic potential and allows us to quantitatively assess the achievable coherence of a vacuum-ultraviolet frequency comb generated through below-threshold harmonics. We find that under reasonable experimental conditions, temporal coherence is maintained. As evidence, we present the first explicit vacuum-ultraviolet frequency-comb structure beyond the third harmonic.

High-repetition-frequency HHG has recently been enabled through the use of femtosecond enhancement cavities[1,2]. In addition to potentially transferring frequency comb techniques[3,4] to the vacuum-ultraviolet range for possible applications such as direct frequency-comb spectroscopy[5–7], the enhancement-cavity technique allows for greater harmonic photon flux and a near-perfect Gaussian fundamental beam, which provides for exceptionally clean and high signal-to-noise studies of the HHG process itself. Here, we use these techniques and present a new set of experimental and theoretical studies of harmonics 7 to 13, generated below and near the ionization threshold in xenon gas with an intense 1,070 nm laser pulse. These harmonic orders are of great interest for the development of vacuum-ultraviolet frequency combs and it is crucial to understand how fluctuations in the driving-laser intensity influence the pulse-to-pulse coherence properties of the train of vacuum-ultraviolet pulses through the nonlinear HHG process. Production of frequency combs through HHG thus requires a systematic understanding of strong-field atomic physics[8–11], but at the same time it provides a good probe for the latter subject.

Surprisingly, we find that harmonics as low as the seventh contain several contributions with different intensity-dependent phases. Our laser system permits a clean observation of interference between these phase contributions at unprecedented signal-to-noise ratios. In particular, we see experimentally a strong contribution from a component that has a large, intensity-dependent phase and we show theoretically that it originates in semi-classical laser-driven continuum dynamics. We demonstrate that this phase is significantly larger than for above-threshold harmonics owing to the influence of the atomic potential on these low-order harmonics. These measurements also provide a quantitative basis to evaluate the long-term temporal coherence of the vacuum-ultraviolet pulse train, a necessary condition for the establishment of a vacuum-ultraviolet frequency comb. Under reasonable experimental conditions, we find that the frequency-comb structure should indeed emerge. To verify this, we demonstrate for the first time coherence between successive pulses in our seventh-harmonic pulse train ($\lambda \approx 153$ nm), which shows a coherence time roughly five orders of magnitude larger than that shown previously[12,13].

For this study, we use a passive optical cavity to enhance a high-power mode-locked femtosecond fibre laser at 1,070 nm. We are able to achieve the peak power necessary for HHG at high repetition frequencies (136 MHz), which gives a very high signal-to-noise ratio and allows the pulse-to-pulse coherence measurements shown later. Figure 1 shows the experimentally measured on-axis yields of harmonics 7 to 13 as a function of the laser intensity in the centre of the gas jet. Interestingly, all four harmonics show complicated intensity-dependent yields, with steep increases interrupted by steps. For harmonics 7 and 11, the intensity steps are more pronounced and occur at lower intensities than for harmonics 9 and 13. The insets show experimentally measured far-field spatial profiles of each harmonic at an intensity of 2×10^{13} W cm^{-2}. At this intensity, harmonics 7 and 11 also show strong off-axis halos in their spatial distributions, whereas 9 and 13 do not. We also note that, in contrast to on-axis, the off-axis intensity-dependent yield shows no interference effects.

The experimental results are very well reproduced by the theoretical calculations (shown in Fig. 1 for comparison) obtained by means of the coupled, non-adiabatic solutions of the time-dependent Schrödinger equation and the wave equation for a gas of xenon atoms exposed to an intense, 1,070 nm laser pulse. Our approach is described in detail in ref. 14, with the important difference that for the work described here we are directly integrating the time-dependent Schrödinger equation numerically within the single-active-electron approximation[15]. We are thus treating the laser electric field and the atomic potential on an equal footing, which is necessary to describe harmonics with photon energies below and close to the ionization threshold. As initial

[1]JILA, National Institute of Standards and Technology, and University of Colorado. Department of Physics, University of Colorado, Boulder, Colorado 80309-0440, USA, [2]Department of Physics and Astronomy, Louisiana State University, Baton Rouge, Louisiana 70803-4001, USA.
*e-mail: Ye@JILA.Colorado.edu.

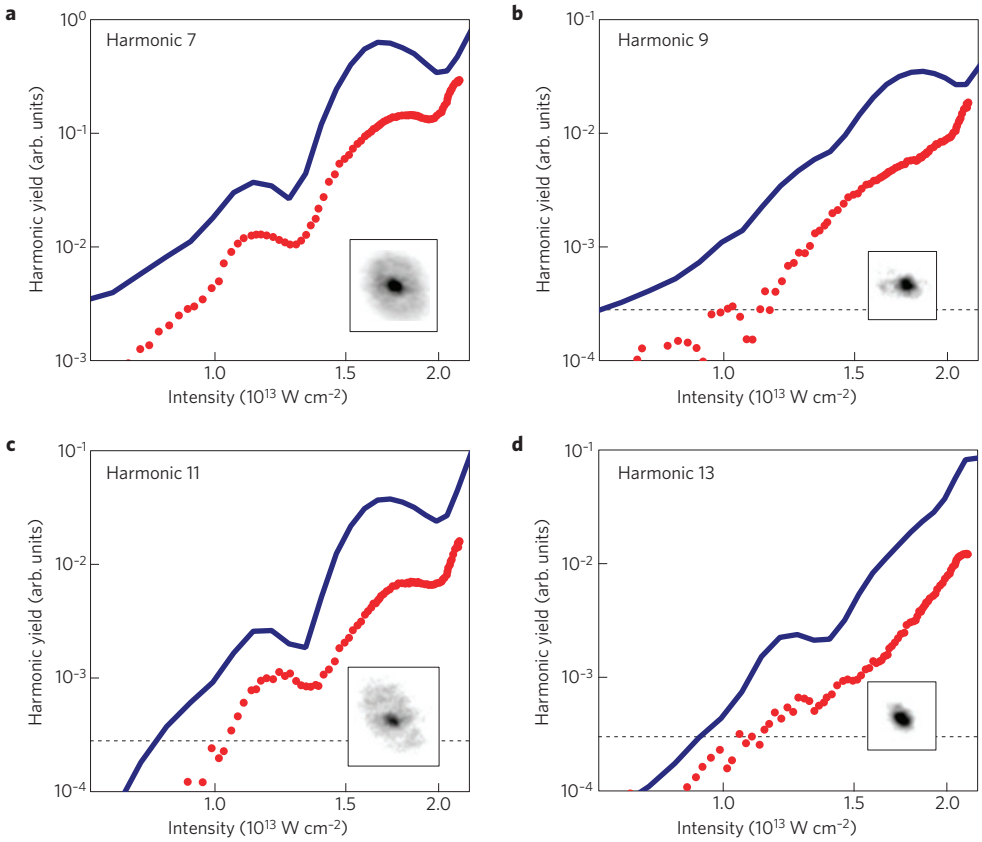

Figure 1 | Harmonic yield as a function of the intensity at the centre of the xenon jet. a–d, Harmonics 7 to 13, respectively. The red filled circles are measured and the blue solid lines are theory (see text), both for the on-axis yield. The harmonic yields are all roughly proportional to the sixth power of the driving intensity. The horizontal dashed lines in **b–d** show the noise floor of the CCD camera. Theoretical harmonic yields were scaled in magnitude to offer a clear comparison. The insets show the far-field spatial profile for each harmonic. Halos on the beam profile and strong oscillations in the intensity-dependent yield are clearly visible in harmonics 7 and 11, providing clear evidence of multiple generation pathways with distinct intensity-dependent phases.

conditions for the calculation, we use the same parameters as the experiment (the calculations are carried out with 50-fs pulses to save computing time; however, we have checked that the results do not change for longer pulses). The theory results reproduce the overall increase of the yield with intensity and show prominent intensity-dependent steps in harmonics 7 and 11, and less pronounced steps in harmonics 9 and 13. Furthermore, the positions of the steps are remarkably well reproduced by theory.

Our experimental and theoretical results suggest that the observed intensity dependence is due to interference between contributions to the harmonic generation process that have different intensity-dependent phases. To explore these different contributions, we analyse the single-atom intensity-dependent dipole moment $d_q(I)$ for each harmonic q in terms of its conjugate-phase variable α, as described in detail in ref. 16. From the calculated dipole phase, we deduce the weight of each contribution, called a quantum path in the literature, over a range of intensities around I_0, by means of the transform:

$$\tilde{d}_q(\alpha, I_0) = \int d_q(I) e^{i\alpha U_p(I)/\hbar\omega} W(I - I_0)\, dI$$

where $W(I - I_0)$ is a window function centred on I_0. The contribution characterized by phase coefficient α_j has a phase that is proportional to the intensity through $\phi_j = \alpha_j U_p(I)/\hbar\omega$, where $U_p = I/4\omega^2$ is the ponderomotive energy in atomic units and ω is the laser frequency. For above-threshold harmonics, the phase coefficients obtained in this way correspond well to those predicted by the semi-classical model[17], including the familiar short and long trajectories with phase coefficients of $\alpha_1 \approx 0.2\pi$ and $\alpha_2 \approx 2\pi$, respectively[18]. To our knowledge, this analysis has not been applied to below-threshold harmonics before.

Figure 2 shows the results of the quantum path analysis for harmonics 7–13 in xenon. All of the harmonics show multiple quantum path contributions; the two dominant ones have phase coefficients $\alpha_0 \approx 0$ and $\alpha_2 \approx 2.5\pi$–3π. To understand the origin of the α_2 contribution to the below-threshold harmonics, we have studied electron trajectories in a generalized semi-classical model in which the atomic potential is present. Crucially, we have found that in the presence of the atomic potential, low-energy electrons can lose enough energy to have less than zero total energy at $x = 0$ (the position of the ion), leading to the emission of below-threshold harmonics. In the tunnel-ionization model, this can happen only for electrons that have followed the long trajectory because they return to x_i, the position of ionization, at a time when the force from the laser field is against their motion. We find that the long trajectories accumulate an intensity-dependent phase that is larger than in the no-potential case, with a phase coefficient close to 3π for the range of intensities we are interested in, rather than the 2π predicted with no potential. This is in good agreement with the result in Fig. 2. There are no negative-energy returns for short-trajectory electrons in the tunnelling model because they return to x_i at a time when the laser field further accelerates them towards $x = 0$. This leads us to designate the α_0 contribution as a multiphoton process with no intensity-dependent phase and not a generalized short trajectory. We note that harmonics 3 and 5 show only an α_0 contribution.

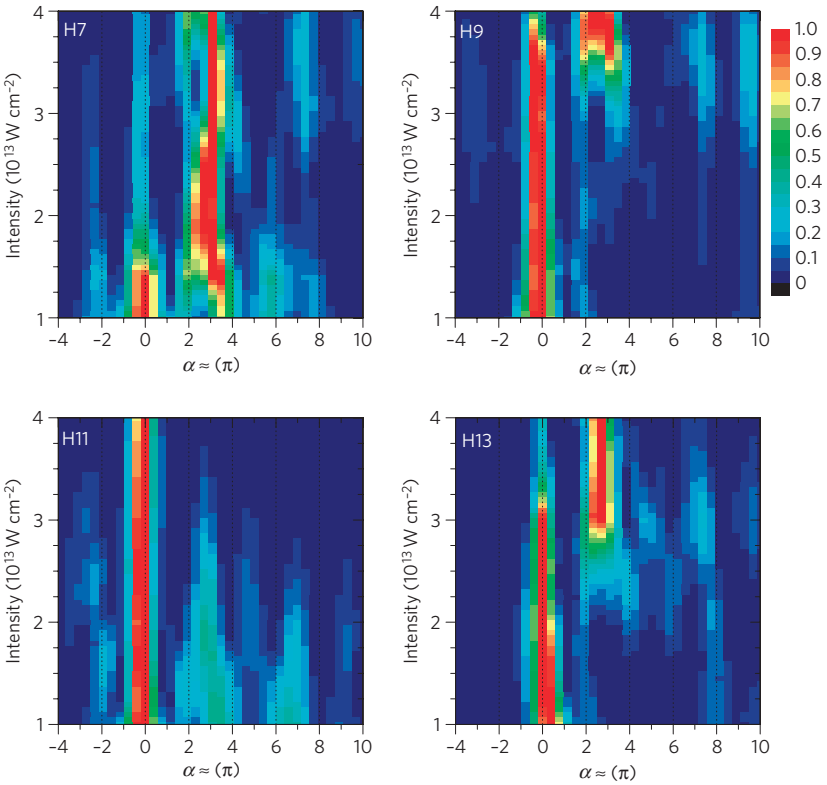

Figure 2 | Quantum path distributions calculated for harmonics 7–13. The colour scale has been normalized for each intensity and shows only relative strengths. Harmonics 7 and 11 show large quantum path contributions at $\alpha \approx 0$ and $\alpha \approx 3\pi$ that manifest themselves in the spatial profiles with halos and intensity-dependent yields with large oscillations, as shown in Fig. 1. Harmonic 9 (13) does not show prominent contributions for $\alpha > 2\pi$ at intensities below $\sim 3 \times 10^{13}$ W cm^{-2} ($\sim 2.5 \times 10^{13}$ W cm^{-2}), so the features indicative of multiple quantum paths are largely absent at the driving intensities present in the experiment.

The calculations in Fig. 2 confirm our interpretation of the experimental results in Fig. 1 as manifestations of the multiple generation mechanisms. The strong halos in the far-field spatial profiles of harmonics 7 and 11 are consistent with a large α_2 contribution to these harmonics at intensities below 2×10^{13} W cm^{-2}. This is because the large intensity-dependent phase, coupled with the Gaussian spatial profile of the fundamental beam, produces a strongly curved harmonic wavefront[19]. For harmonics 9 and 13, the α_2 contribution in Fig. 2 is significant only at the upper range of intensities used in this experiment. As an experimental confirmation, we observe the sudden appearance of a halo on harmonic 9 at our highest experimental intensity. This reveals that the seemingly distinct behaviour of harmonics 9 and 13 arises mainly from the higher intensity threshold necessary to observe a large α_2 contribution. Although several generation pathways are familiar from HHG high above the ionization threshold, it has never been observed (or predicted) so far below threshold. Previous works have noted that harmonics close to threshold can have large intensity-dependent phases[20] and that harmonics well below threshold can show a step in the intensity-dependent yield, which was interpreted as an atomic resonance effect[21]. Our results explain and extend these observations to harmonics well below and around threshold without invoking atomic resonances. As it turns out that the intensity dependence of the dipole phase below threshold is due primarily to continuum dynamics, we have now a general quantitative connection between the laser intensity and the phase for these harmonics.

The observation of a large intensity-dependent phase contribution to harmonics as low as the seventh in our experiment allows us to connect these measurements to several other strong-field phenomena observed in recent years. These experiments, which measured ionization dynamics rather than photon emission, all invoke motion in the combined field of the ion and laser field to explain the behaviour of electrons with energies below the ionization threshold. Ho and Eberly studied non-sequential double ionization by means of classical simulations and found that trajectories for which an ionized electron was slowed down as it approached the ion significantly enhanced the *e*–*e* interaction that leads to double ionization[22]. Recently, Nubbemeyer, *et al.* found an unexpectedly large fraction of excited neutral atoms surviving a strong laser pulse[23]. Their explanation, supported by classical simulations, invokes tunnel-ionization trajectories very similar to those we discuss here. Finally, Shuman *et al.* have studied multiphoton-assisted recombination, where an ionized electron exchanges momentum with the laser field in the presence of the Coulomb potential and reattaches to the ion[24]. Our observations and the high dynamic range associated with them, open the possibility to study the electron dynamics invoked in these experiments directly by means of the HHG process.

As the HHG process is extremely nonlinear, it has been a significant concern that frequency-comb coherence could not be maintained through HHG. Previous experiments have measured the coherence maintained in HHG but only over the timescale of a single pulse[12,13]. However, to produce a frequency comb, it is a prerequisite that coherence is maintained between successive pulses in the train as this sets the frequency-comb linewidth to be less than the repetition frequency. This comb linewidth determines the ultimate frequency resolution for experiments using the vacuum-ultraviolet frequency comb[5]. The α parameters discussed above are a direct measure of the intensity-to-phase noise conversion in the below-threshold generation process that is directly relevant to the linewidth of a vacuum-ultraviolet frequency-comb mode. For

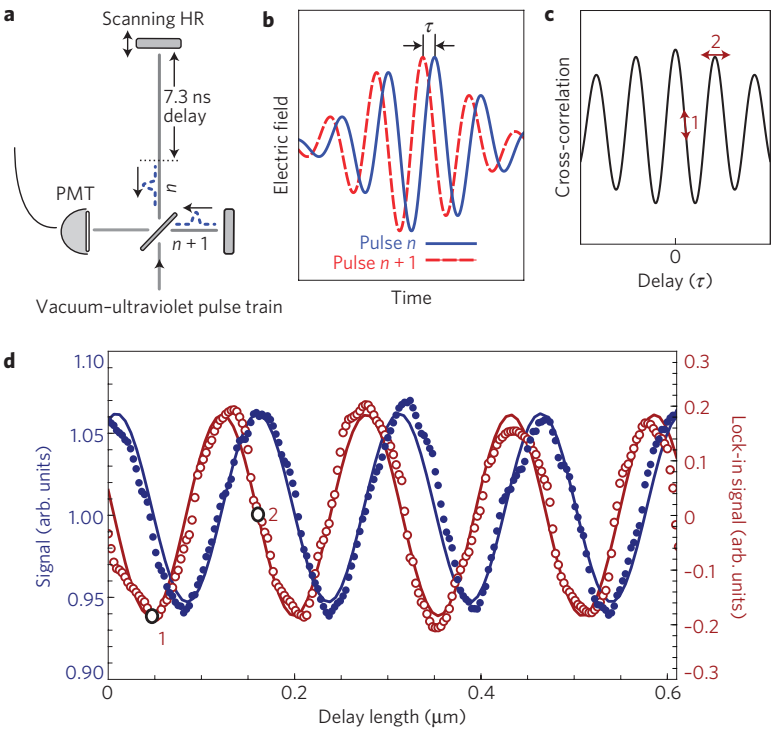

Figure 3 | Seventh-harmonic pulse-to-pulse coherence measurement. a, Pulse-to-pulse measurement set-up: a vacuum-ultraviolet interferometer with the delay set for pulse n in the seventh-harmonic pulse train to interfere with pulse $n+1$. HR: high reflector. **b**, The electric field of pulse n in the seventh-harmonic pulse train that has been sent through an optical delay line so that it interferes with the $n+1$ pulse in the train, which is shown as the dashed red trace. **c**, A cross-correlation signal results as the length of the delay line is scanned. **d**, The blue filled circles show our experimental measurement of the cross-correlation as the path length of the interferometer is linearly scanned, showing a contrast ratio of ≈6% limited by the spatial-mode overlap and the power imbalance between the two interfering pulses. The red open circles show the signal achieved from a lock-in detection of a 392 kHz modulation of the delay line. Both sets of data are fitted with sinusoidal functions. Point 1 in **c** and **d** shows the positions of a maximum negative lock-in signal where the cross-correlation signal at d.c. has a maximum negative slope. Point 2 shows the position of a zero lock-in signal with the d.c. cross-correlation at its maximum.

Table 1 | Frequency-comb parameters for below-threshold harmonics ($\hbar\omega < I_p$) at an intensity of $I = 2 \times 10^{13}$ W cm^{-2} and for above-threshold harmonics ($\hbar\omega > I_p$) at $I = 2 \times 10^{14}$ W cm^{-2}.

	$\hbar\omega < I_p$		$\hbar\omega > I_p$	
Trajectory	$j=0$	$j=2$	$j=1$	$j=2$
α	0.2π	2.7π	0.2π	2π
$\phi_{r.m.s.}$ (rad)	0.01	0.16	0.12	1.16
Carrier power (%)	99.99	97.59	98.67	26.08

Also listed are the r.m.s. phase noise ($\phi_{r.m.s.}$) and an estimate of the power left in a 1 kHz carrier for an individual frequency-comb mode with 1% integrated intensity noise in frequencies above 1 kHz in a $1/f$ distribution.

instance, using α parameters extracted from the experiment, we can estimate the percentage of the power that would be removed from individual 1-kHz-linewidth comb modes for a laser source with a 1% r.m.s. intensity fluctuation with a characteristic $1/f$ distribution for each of the generation processes[25]. The results are presented in Table 1. For comparison, we include α and phase values for harmonics produced high above the ionization threshold, for instance in argon at an intensity of 2×10^{14} W cm^{-2}.

Our estimates of the intensity-to-phase noise put firm limits on the intensity noise that can be tolerated to preserve the comb structure in HHG and it is clear from Table 1 that a very high degree of pulse-to-pulse coherence should be possible in principle. To put this question to rest, we demonstrate pulse-to-pulse coherence of the seventh harmonic. For this study, the harmonic radiation is collimated and sent through a cross-correlation interferometer with a delay set so that a pulse in the harmonic train will interfere with the subsequent pulse, allowing us to measure the degree of pulse-to-pulse coherence[26]. As the seventh-harmonic radiation is absorbed in air and most solid materials, extreme care was taken in the design and construction of this interferometer, with all necessary optical alignments being conducted under vacuum.

Figure 3 shows the interference signal as the path length of the interferometer was scanned over 600 nm in about 2 s. The pulse-to-pulse coherence is clearly visible in the figure as a cross-correlation that corresponds to the seventh-harmonic wavelength of ≈150 nm. The contrast ratio shown in the figure is only ≈6%; however, if we take into account imperfect collimation and severe power imbalance in the interferometer, we estimate that the maximum achievable contrast ratio was 10–15%. To provide a zero background for a significantly enhanced measurement contrast, we also used a lock-in detection by dithering the length of the interferometer at 392 kHz as the length of the interferometer was scanned. The demodulated signal is also shown in Fig. 3.

As imperfect alignment in the interferometer and pulse overlap can easily decrease the contrast ratio further, our measurement provides only a lower bound on the coherence. By measuring the pulse-to-pulse coherence, we place a lower bound on the coherence time (∼10 ns), which is roughly five orders of magnitude longer than that measured before[12,13]. The corresponding frequency-comb linewidth is narrower than 20 MHz.

We have found experimental and theoretical evidence for multiple contributions to the generation of below-threshold

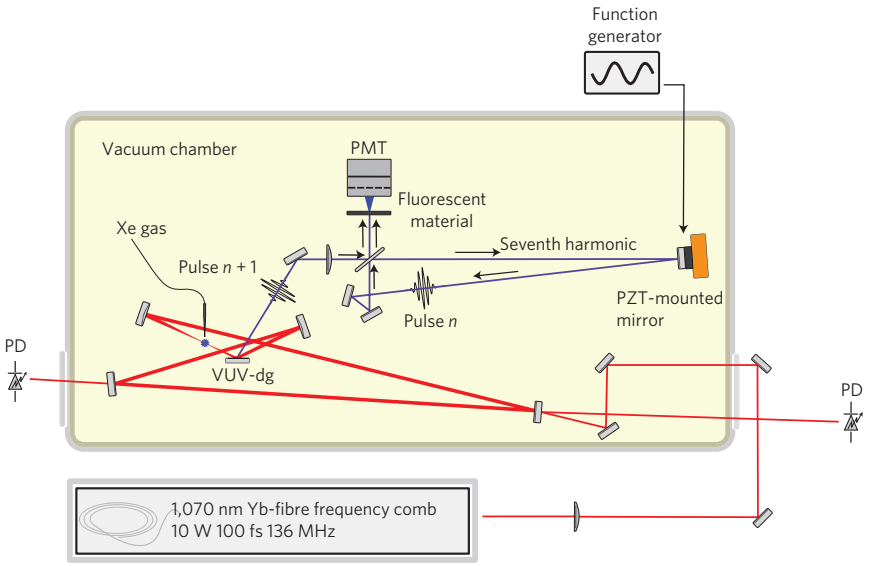

Figure 4 | Experimental set-up for the demonstration of vacuum-ultraviolet pulse-to-pulse coherence. A cavity-enhanced Yb-fibre frequency comb is used to generate harmonics in xenon gas. Photodiodes (PD) are used to monitor the reflected and transmitted fundamental light and maintain resonance between the frequency comb and the enhancement cavity[1,2]. An intracavity vacuum-ultraviolet diffraction grating (VUV-dg) is used to outcouple the seventh-harmonic radiation[29], which is then sent through a cross-correlation interferometer. One mirror in the delay arm of the interferometer is mounted on a PZT, allowing scans of the differential path length. The seventh-harmonic radiation at the output of the interferometer is detected by monitoring the fluorescence from a sodium-salicylate-coated plate with a PMT.

harmonics. In particular, one of these contributions is dominated by laser-driven continuum dynamics, in analogy with the semi-classical model for generation of high-order harmonics. Our measurements of the spatial and spectral profiles and of the intensity dependence of the interference pattern all confirm that the intensity-dependent phase is larger for these low-order harmonics than for high-order harmonics owing to the influence of the atomic potential. We used our measured phase coefficients to estimate the coherence one can expect in both low-order and high-order harmonic frequency combs and demonstrated that indeed, pulse-to-pulse coherence was maintained for the below-threshold harmonic generation.

Methods

The enhancement cavity. To excite the enhancement cavity, we use a high-powered, frequency-controlled 1,070 nm fibre laser system that supplies 100-fs pulses at 136 MHz with a pulse energy of 75 nJ (refs 27, 28). When the pulse train is resonant with the cavity (obtained by actively controlling the two independent degrees of freedom of the frequency comb, the repetition frequency and the offset frequency), we achieve an enhancement of 260, which translates to an intracavity pulse energy of 19 μJ. Two 10-cm radius-of-curvature mirrors within the cavity produce a focal spot area of 960 μm^2 that yields a peak intensity of 4×10^{13} W cm^{-2}. To generate harmonic radiation, we inject xenon gas near the intracavity focus using a glass nozzle with a 100 μm aperture and a backing pressure of 425 torr. An extreme-ultraviolet diffraction grating is used as one element of the enhancement cavity so that a portion of the harmonic radiation generated diffracts out of the cavity and impinges on a fluorescent plate[29]. By imaging the fluorescence onto a CCD (charge-coupled device) camera, we are able to make measurements of the power and far-field profile for individual harmonics. To rule out possible effects from nonlinear responses of the detection scheme (the combination of sodium salicylate with a CCD camera), we retook the experimental data shown in Fig. 1 with a decreased pressure of xenon gas that resulted in an order of magnitude decrease in the harmonic flux. The essential features in Fig. 1 (the slopes and oscillations) were minimally affected, ruling out the possibility of any significant detection nonlinearity.

Intensity calibration. The peak power within the enhancement cavity was determined accurately by measuring the average power within the enhancement cavity and the pulse duration of the driving field. The average power within the cavity was determined by monitoring the transmitted light through one cavity mirror for which the transmission was well calibrated and the pulse duration was determined by autocorrelation of the transmitted light. As the enhancement cavity defines the resonant spatial mode, the mode volume at the focus can be determined accurately by a simple calculation. Together with the determination of the peak power, this calculation provides a dependable calibration of the peak intensity within the enhancement cavity.

The use of an optical cavity ensures that the spatial profile of the optical cavity field is well defined, power independent and can be precisely determined. The beam profile of the transmitted fundamental radiation was measured and found to be a near-perfect TEM_{00} as a result of the transverse-mode filtering provided by the enhancement cavity. This mode structure is maintained at the intracavity focus so that we can be confident that the harmonics were being generated by a high-quality TEM_{00} beam. The exact location of the experimental laser focus relative to the gas jet, which is known only to within 200 μm, is inferred by aligning the experimental and theoretical result at the lowest intensity step for harmonic 7. This results in all of the intensity-step positions being remarkably consistent between theory and experiment.

Experimental determination of phase-coefficient values. To extract values for the phase coefficients α_0 and α_2 shown in Table 1, we made careful measurements of the inner and outer parts of the spatial (or spectral) profile of harmonic 7 at a well-known intensity[30]. If we assume that the harmonic has a Gaussian spatial (temporal) profile with an extra intensity-dependent phase and a focal spot (duration) that is one half of the infrared spot (pulse), we find $\alpha_2 \approx 2.7\pi$ and $\alpha_0 \leq 0.2\pi$. Likewise, using the intensity separation between the two prominent steps in Fig. 1 as the 'period' of the interference between the two contributions, we extract a value of $\alpha_2 - \alpha_0 \approx 3\pi$ (ref. 31). All three of these measurements are thus in excellent agreement with the theoretical predictions.

Coherence measurements. For the pulse-to-pulse coherence measurements, the harmonic radiation outcoupled with the intracavity diffraction grating was sent through a vacuum-ultraviolet interferometer (see Fig. 4). A MgF_2 beam splitter, calcium fluoride lenses and aluminium mirrors optimized for operation in the vacuum-ultraviolet were used for the construction of the interferometer. As the reflectivity of the MgF_2 beam splitter was only due to the Fresnel reflection (0.09 for 152 nm light and S polarization), the ratio of power in the two arms was ≈0.12. One end-mirror of the interferometer was mounted on a piezoelectric transducer (PZT) so that the optical delay of the interferometer could be scanned and quickly modulated. To detect radiation at the output port, we used a conventional photomultiplier tube (PMT) with a thin layer of sodium salicylate on the front surface. The sodium salicylate fluoresces at a wavelength of about 420 nm when struck by the seventh-harmonic radiation, which matches very well to the peak detection efficiency of the PMT. To observe the interference with a better contrast, we applied a 392 kHz modulation to the PZT. The PZT and mounted mirror had a natural resonance close to this frequency, allowing enhanced mirror travel. The demodulated signal is basically the first-order derivative of the d.c.-based interference measurement.

Received 8 June 2009; accepted 14 August 2009; published online 20 September 2009

References

1. Jones, R. J., Moll, K. D., Thorpe, M. J. & Ye, J. Phase-coherent frequency combs in the vacuum ultraviolet via high-harmonic generation inside a femtosecond enhancement cavity. *Phys. Rev. Lett.* **94,** 193201 (2005).
2. Gohle, C. *et al.* A frequency comb in the extreme ultraviolet. *Nature* **436,** 234–237 (2005).
3. Cundiff, S. T. & Ye, J. Femtosecond optical frequency combs. *Rev. Mod. Phys.* **75,** 325–342 (2003).
4. Udem, T., Holzwarth, R. & Hänsch, T. W. Optical frequency metrology. *Nature* **416,** 233–237 (2002).
5. Marian, A., Stowe, M. C., Lawall, J. R., Felinto, D. & Ye, J. United time-frequency spectroscopy for dynamics and global structure. *Science* **306,** 2063–2068 (2004).
6. Witte, S., Zinkstok, R. Th., Ubachs, W., Hogervorst, W. & Eikema, K. S. E. Deep-ultraviolet quantum interference metrology with ultrashort laser pulses. *Science* **307,** 400–403 (2005).
7. Zinkstok, R. Th., Witte, S., Ubachs, W., Hogervorst, W. & Eikema, K. S. E. Frequency comb laser spectroscopy in the vacuum-ultraviolet region. *Phys. Rev. A* **73,** 061801 (2006).
8. Lewenstein, M., Balcou, Ph., Ivanov, M. Y., L'Hullier, A. & Corkum, P. B. Theory of high-harmonic generation by low-frequency laser fields. *Phys. Rev. A* **49,** 2117–2132 (1994).
9. Meckel, M. *et al.* Laser-induced electron tunneling and diffraction. *Science* **320,** 1478–1482 (2008).
10. Hentschel, M. *et al.* Attosecond metrology. *Nature* **414,** 509–513 (2001).
11. Sansone, G. *et al.* Isolated single-cycle attosecond pulses. *Science* **314,** 443–446 (2006).
12. Lyngå, C. *et al.* Temporal coherence of high-order harmonics. *Phys. Rev. A* **60,** 4823–4830 (1999).
13. Cavalieri, S., Eramo, R., Materazzi, M., Corsi, C. & Bellini, M. Ramsey-type spectroscopy with high-order harmonics. *Phys. Rev. Lett.* **89,** 133002 (2002).
14. Gaarde, M. B., Tate, J. L. & Schafer, K. J. Macroscopic aspects of attosecond pulse generation. *J. Phys. B* **41,** 132001 (2008).
15. Schafer, K. J. & Kulander, K. C. High harmonic generation from ultrafast pump lasers. *Phys. Rev. Lett.* **78,** 638–641 (1997).
16. Balcou, Ph., Dederichs, A. S., Gaarde, M. B. & L'Huillier, A. Quantum-path analysis and phase matching of high-order harmonic generation and high-order frequency mixing processes in strong laser fields. *J. Phys. B* **32,** 2973–2989 (1999).
17. Gaarde, M. B. & Schafer, K. J. Quantum path distributions for high-order harmonics in rare gas atoms. *Phys. Rev. A* **65,** 031406(R) (2002).
18. Lewenstein, M., Salières, P. & L'Huillier, A. Phase of the atomic polarization in high-order harmonic generation. *Phys. Rev. A* **52,** 4747–4754 (1995).
19. Bellini, M. *et al.* Temporal coherence of ultrashort high-order harmonic pulses. *Phys. Rev. Lett.* **81,** 297–300 (1998).
20. Peatross, J. & Meyerhofer, D. Angular distribution of high-order harmonics emitted from rare gases at low density. *Phys. Rev. A* **51,** R906–R909 (1995).
21. Balcou, Ph. & L'Huillier, A. Phase matching effects in strong-field harmonic generation. *Phys. Rev. A* **47,** 1447–1459 (1993).
22. Ho, P. J. & Eberly, J. H. Different rescattering trajectories related to different total electron momenta in nonsequential double ionization. *Opt. Express* **11,** 2826–2831 (2003).
23. Nubbemeyer, T., Gorling, K., Saenz, A., Eichmann, U. & Sandner, W. Strong-field tunneling without ionization. *Phys. Rev. Lett.* **101,** 233001 (2008).
24. Shuman, E. S., Jones, R. R. & Gallagher, T. F. Multiphoton assisted recombination. *Phys. Rev. Lett.* **101,** 263001 (2008).
25. Zhu, M. & Hall, J. L. Stabilization of optical phase/frequency of a laser system: Application to a commercial dye laser with an external stabilizer. *J. Opt. Soc. Am. B* **10,** 802–816 (1993).
26. Xu, L. *et al.* Route to phase control of ultrashort light pulses. *Opt. Lett.* **21,** 2008–2010 (1996).
27. Hartl, I. *et al.* Cavity-enhanced similariton Yb-fiber laser frequency comb: 3×10^{14} W cm^{-2} peak intensity at 136 MHz. *Opt. Lett.* **32,** 2870–2872 (2007).
28. Schibli, T. R. *et al.* Optical frequency comb with submillihertz linewidth and more than 10 W average power. *Nature Photon.* **2,** 355–359 (2008).
29. Yost, D. C., Schibli, T. R. & Ye, J. Efficient output coupling of intracavity high-harmonic generation. *Opt. Lett.* **33,** 1099–1101 (2008).
30. He, X. *et al.* Spatial and spectral properties of the high-order harmonic emission in argon for seeding applications. *Phys. Rev. A* **79,** 063829 (2009).
31. Zaïr, A. *et al.* Quantum path interferences in high-order harmonic generation. *Phys. Rev. Lett.* **100,** 143902 (2008).

Acknowledgements

We gratefully thank I. Hartl, A. Marcinkevičius and M. Fermann at IMRA America, for the design and construction of the high-power Yb-fibre laser system. Funding at JILA is provided by DARPA, NIST and NSF. Funding at LSU is provided by the NSF through grant numbers PHY-0449235 and PHY-0701372, and by the CCT at LSU. K.J.S. acknowledges support from the Ball Family Professorship. Portions of this research were conducted with high-performance computational resources provided by the Louisiana Optical Network Initiative (http://www.loni.org).

Author contributions

The experimental work was carried out by the team at JILA: D.C.Y., T.R.S. and J.Y. The theoretical work was carried out by the team at LSU: J.L.T., J.H., M.B.G. and K.J.S. Manuscript preparation was completed by D.C.Y, J.Y., M.B.G. and K.J.S.

Additional information

Reprints and permissions information is available online at http://npg.nature.com/reprintsandpermissions. Correspondence and requests for materials should be addressed to J.Y.